
Fractography of Advanced Ceramics II

Edited by

J. Dusza, R. Danzer and R. Morrell

ttp TRANS TECH PUBLICATIONS

Fractography of Advanced Ceramics II

Edited by
J. Dusza
Prof. Robert Danzer
Roger Morrell

Fractography of Advanced Ceramics II

Proceedings of the 2nd International Conference on
Fractography of Advanced Ceramics, held in Stará Lesná,
Slovakia, October 3-6, 2004

Edited by

J. Dusza, Prof. Robert Danzer and Roger Morrell

■ *Scientific.Net* ■

Copyright © 2005 Trans Tech Publications Ltd, Switzerland

All rights reserved. No part of the contents of this publication may be reproduced or transmitted in any form or by any means without the written permission of the publisher.

Trans Tech Publications Ltd
Kapellweg 8
CH-8806 Baech
Switzerland
<https://www.scientific.net>

Volume 290 of
Key Engineering Materials
ISSN print 1013-9826
ISSN web 1662-9795

Full text available online at <http://www.scientific.net>

Distributed worldwide by

Trans Tech Publications Ltd
Kapellweg 8
CH-8806 Baech
Switzerland
Phone: +41 (44) 922 10 22
Fax: +41 (44) 922 10 33
e-mail: sales@scientific.net

Table of Contents

Machining Cracks in Finished Ceramics G.D. Quinn, L.K. Ives and S. Jahanmir	1
Edge Flaking - Similarity between Quasistatic Indentation and Impact Mechanisms for Brittle Materials R. Morrell	14
Effect of Indenter Materials on Indentation Fracture of Alumina Ceramics H. Usami, T. Kadomae, D. Igimi and M. Mizuno	23
Scratchability of Soda-Lime Silica (SLS) Glasses: Dynamic Fracture Analysis V. Le Houérou, J.-. Sanglebœuf and T. Rouxel	31
Fracture Toughness of Ceramic Materials and Its Relationship to Chipping Formation Z. Jonšta, J. Horváthová, K. Blažková and K. Mazanec	39
Strength and Fractography of Piezoceramic Multilayer Stacks P. Supancic, Z. Wang, W. Harrer, K. Reichmann and R. Danzer	46
Thermography and Simulation as a Combined Method for Failure Analysis of PTCs A. Platzer, P. Supancic, C. Lembacher, U. Theiszl and R. Danzer	54
Fracture Origins in Miniature Silicon Carbide Structures G.D. Quinn, W.N. Sharpe, G.M. Beheim, N.N. Nemeth and O. Jadaan	62
Nanofractography of Alumina by Scanning Probe Microscopy J. Tatami, T. Ohbuchi, K. Komeya and T. Meguro	70
Failure Analysis on a De-NO_x Catalyst of a Large Waste Burner J. Kübler, R. Baechtold, G. Blugan, K. Lemster and S. Fuso	78
Damage Growth in Porous Ceramics T. Sadowski, S. Samborski and Z. Librant	86
Failure Analysis of Si₃N₄ Rolls for Wire Hot Rolling by Numerical Simulation of Thermal and Mechanical Stresses M. Lengauer, R. Danzer, D. Rubeša, W. Harrer and W. Zleppnig	94
Contact Strength of the RE-Oxynitride Glasses F. Lofaj and F. Dorčáková	102
Fracture and Fatigue Behaviour of Mullite/Molybdenum Composites Y. Torres Hernández, M. Anglada, L. Llanes, J.F. Bartolomé, M. Díaz and J.S. Moya	110
Polymer-Derived Al₂O₃-SiC Nanocomposites: Preparation Route vs. Microstructure D. Galusek, R. Riedel and M. Balog	121
Fracture Toughness Enhancements through Stress Shielding in Functionally Graded SiC-TiC Composites J.H. Liversage, D.S. McLachlan and M. Herrmann	129
Development of Preparation Processes for CNT/Si₃N₄ Composites C. Balázsi, F. Wéber, Z. Kövér, Z. Kónya, I. Kiricsi, L.P. Biró and P. Arató	135
Fracture and Crystallographic Phase Correlation in Alumina Based Particulate Composites Z. Pędzich and M. Faryna	142
Quantitative Surface Fractography of Alumina and Alumina-SiC Composites during Diamond Grinding J.L. Ortiz Merino, A. Cock, S.G. Roberts and R.I. Todd	149
Effect of Carbon and Nitrogen Implantation on the Properties of Silicon Nitrides P. Arató, C. Balázsi, Z. Kövér, F. Wéber, E. Richter and J. Gyulai	160
Fracture Resistance Evaluation of Fibre Reinforced Brittle Matrix Composites I. Dlouhý and Z. Chlup	167
Failure Behaviour of High Toughness Multi-Layer Si₃N₄ and Si₃N₄-TiN Based Laminates G. Blugan, R. Dohedoe, I. Gee, N. Orlovskaya and J. Kübler	175
Interfacial Fracture Toughness Measurement of Thick Ceramic Coatings by Indentation M. Bartsch, I. Mircea, J. Suffner and B. Baufeld	183
Thermal Shock Behavior of an Al₂O₃/ZrO₂ Multilayered Ceramic with Residual Stresses due to Phase Transformations R. Bermejo, L. Llanes, M. Anglada, P. Supancic and T. Lube	191

Failure Mechanisms in Directionally Solidified Alumina-Titania Composites C. Baudín, A. Sayir and M.H. Berger	199
Fracture of Monoliths Fabricated by Stacking Water Processed Green Ceramic Tapes J. Gurauskis, J. Pascual, T. Lube, A.J. Sanchez-Herencia and C. Baudín	203
Fracture Mechanisms in Laminates in the Alumina - Titania System S. Bueno and C. Baudín	208
R-Curves in Al_2O_3 - $\text{Al}_2\text{O}_3/\text{ZrO}_2$ Laminates J. Pascual, F. Chalvet, T. Lube and G. de Portu	214
Contact Fatigue in Ceramic Laminated Composites L. Ceseracciu, F. Chalvet, E. Jiménez-Piqué, M. Anglada and G. de Portu	222
Carbon Nanotubes Prepared by CVD Š. Kavecký and P. Šajgalík	230
Effect of Ion-Implantation on the Microstructure of Si_3N_4 Based Ceramics J.K. Babcsán, M.B. Maros, N. Wanderka, D. Klaffke and H. Schubert	234
Size Effects in Micro- and Nanocarbon Added C/Si_3N_4 Composite Prepared by Hot Pressing C. Balázs, F.Ç. Şahin, O. Addemir, Z. Kasztovszky, Z. Kövér and F. Wéber	238
Comparison of Silicon Nitrides with Carbon Additions Prepared by Two Different Sintering Methods C. Balázs, E. Dolekcekcic, Z. Kövér, F. Wéber, S. Hampshire and P. Arató	242
Effect of Rare Earth Oxide and Rare Earth-Alumina-Silica Glass on Mechanical Properties of Liquid Phase Sintered Alumina Ceramics J. Sedláček, D. Galusek and P. Šajgalík	246
Mechanical Properties and Microstructure of α-SiAlON Based Cutting Tools D. Salamon, P. Šajgalík and M. Liška	250
Influence of Alumina Platelets on the Mechanical Strength of Porous Zirconia Tape Z.S. Rak	254
Thermal Shock Resistance of Cordierite-Mullite Refractory Composites Z. Chlup, I. Dlouhý, A.R. Boccaccini, D.N. Boccaccini, C. Leonelli and M. Romagnoli	260
Residual Stresses in Al_2O_3-ZrO_2 Laminar System P. Zimovčák, T. Köves, J. Dusza, F. Chalvet and G. de Portu	264
Structure of Post-Creep Carbon Fibres H. Rennhofer, D. Loidl, J. Brandstetter, K. Kromp, R. Weiss and H. Peterlik	268
Nano-Indentation of SiC and $\text{Si}_3\text{N}_4/\text{SiC}$ Ceramic Materials M. Balog, P. Šajgalík, Z. Lenčes, M. Hnatko, J. Kečkéš, J.L. Huang, J. Janega and R. Horváthová	272
A Contribution of Fractal Geometry to Characterization of Wear Process M. Kupková, M. Kupka, E. Rudnayová and J. Dusza	276
Fractographic Studies of Sapphire Fibers Using Laser Scanning Confocal Microscopy J.M. López-Cepero, J.J. Quispe Cancapa, A.R. de Arellano-López and J. Martínez-Fernández	280
Study on New Ceramic Coated Metal Powders: Microstructure and Properties M. Actis Grande, R.M. Piticescu, C. Bogdanescu, M. Rosso and D. Ugues	284
Indentation Testing of MoSi_2 M. Henžel, P. Zimovčák, J. Dusza, A. Juhász and J. Lendvai	288
Labeled Weibull Plot of a C-Derived Si_3N_4-SiC Nanocomposite M. Kašiarová, J. Dusza, M. Hnatko and P. Šajgalík	292
Thermal Shock Resistance of the RE-Oxide and Oxynitride Glasses F. Lofaj and F. Dorčáková	296
Fractographic Analysis of Surface Flaws in Glass M. Kašiarová, T. Rouxel, J.-. Sangleboeuf and V. Le Houérou	300
Determination of Dynamic Fracture Toughness of Si_3N_4 Ceramics by Instrumented Impact Test M.B. Maros, N.K. Helmecci, B.G. Lenkey and P. Arató	304
Determination of Fracture Toughness and Fracture Probability of LPS Aluminas by Hertzian Indentation D. Galusek, F.L. Riley and M. Liška	308
Low Cost SiAlON from Pyrophyllite with High Hardness and Good Corrosion Resistance J. Křest'an, P. Šajgalík, Z. Pánek and D. Salamon	312
Indentation Testing of an $\text{Al}_2\text{O}_3/\text{Al}_2\text{O}_3 + \text{ZrO}_2$ Layered Composite P. Zimovčák, T. Köves, J. Dusza, L. Pešek, F. Chalvet and G. de Portu	316

Thermal Stresses in SiC-Si₃N₄ Cubic-Cell-Divided Multi-Particle-Matrix System L. Ceniga	320
Fracture Behaviour of Pressureless Sintered Nickel-Reinforced Alumina Composites A. Beverina, A.J. Sanchez-Herencia, N. Hernández and R. Moreno	324
Residual Stress Profile Determined by Piezo-Spectroscopy in Alumina/Alumina-Zirconia Layers Separated by a Compositionally Graded Intermediate Layer M. Popa, J. Calderón Moreno, P. Hvizdoš, R. Bermejo and G. Anné	328
Mechanical Properties of Alumina/Zirconia Functionally Graded Material Prepared by Electrophoretic Deposition P. Hvizdoš, J. Calderón Moreno, J. Očenášek, L. Ceseracciu and G. Anné	332
Mechanical Properties of Thermal Barrier Coatings at Room Temperature G. Guidoni, Y. Torres Hernández and M. Anglada	336
Effect of Oxidation at Elevated Temperature on Elastic and Interface Properties of Ceramic Matrix Composites J. Brandstetter, P. Glogar, D. Loidl and K. Kromp	340
Mechanical and Fracture Properties of R-Glass Reinforced Composites with Pyrolysed Polysiloxane Resin as a Matrix M. Černý, D. Bednářová, P. Glogar, J. Dusza and E. Rudnayová	344
The Preparation and Properties of Functionally Graded Alumina/Zirconia-Toughened Alumina (ZTA) Ceramics for Biomedical Applications S. Beranič Klopčič, S. Novak, T. Kosmač, H.G. Richter and S. Hecht-Mijic	348
PZT Ceramics Prepared from Two Phase Gels J. Briančin, L. Medvecký, H. Bruncková and M. Kmecová	353
Strength and Fractography of High Power Varistors Z. Wang, P. Supancic, F. Aldrian, A. Schriener and R. Danzer	358
Delayed Fatigue of Hydroxy- and Fluorhydroxyapatite Ceramics in Simulated Body Fluid S.M. Barinov, I.V. Fadeeva, L.V. Fateeva and S.V. Tumanov	366
Fracture Characteristic of Isostatic Pressed Submerged Entry Nozzle A. Mašlejová and A. Leško	370

George D. Quinn,^a Lewis K. Ives^b and S. Jahanmir^c
National Institute of Standards and Technology, Ceramics Division, Stop 852,
Gaithersburg, MD, 20899, USA
^ageorge.quinn@nist.gov, ^blewis.ives@nist.gov, ^csjahanmir@mitiheart.com

Keywords: Fractography, machining cracks, surface flaws, grinding cracks, silicon nitride

Abstract. Grinding may create flaws that control strength and limit the performance of finished ceramics. Machining cracks sometimes have been difficult or impossible to find especially in toughened ceramics with interlocking grain microstructures that create rough fracture surfaces. Our fractographic examinations show that machining damage leaves telltale markings on fracture surfaces that may be easily detected using common fractographic techniques. A comprehensive study with over 400 ground rods and rectangular bars was conducted on several commercial silicon nitrides to study the effects of various machining conditions. Similarities and differences in behavior were observed. A paradoxical finding was that tougher silicon nitrides developed deeper grinding cracks. Machining crack size and shape strongly depended on the grinding wheel grit size.

Introduction

Residual surface cracks from the grinding process may act as strength limiting flaws. **Fig. 1** shows one depiction of these machining cracks and **Fig. 2** shows how the grinding direction can influence the strength. Long coplanar or offset parallel cracks are more deleterious to strength than orthogonal cracks. The difference in size and severity of these cracks causes the strength dependence with orientation, but only if machining cracks control strength. Surface grinding is often done in several stages to limit the damage. Rough and intermediate grinding is done with coarse or medium grit wheels and aggressive removal rates to bring the part close to final dimensions. Finish machining removes the prior damage and obtains correct final part dimensions and finish.

The present study was initiated as part of a program to investigate machining damage in ground ceramics [1,2,3,4,5,6]. Many studies have investigated the effects of surface grinding on flexure strength, but most studies do not include a detailed characterization of the machining flaws such as their size, shape, and morphology, and density. Notable exceptions to this approach have been the studies of Hollstein et al. [7]; Rice, Mecholsky and colleagues [8,9,10,11]; and Foley, Pujari and colleagues [12,13]. Nonetheless, very little work has been done to systematically correlate the size and severity of machining cracks to the grinding conditions that created them.

Fig. 1 Schematic of flaws introduced by machining or scratching a ceramic or glass surface. Adapted from a figure by Rice and Mecholsky [8].

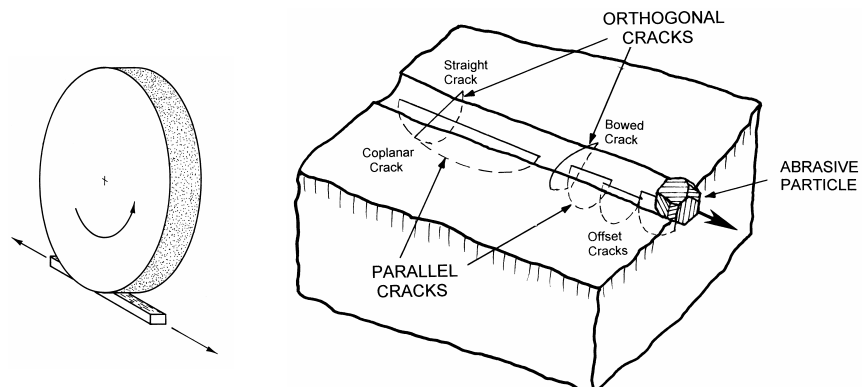
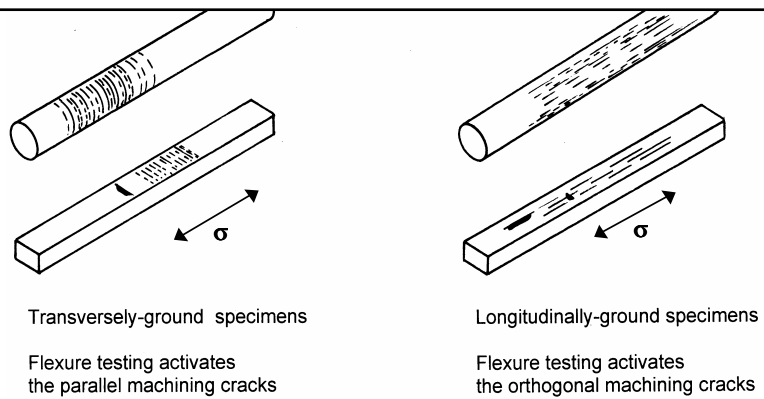


Fig. 2 The grinding direction influences strength.



Machining cracks are relatively easy to detect in homogeneous materials such as glasses, single crystals, very fine-grained fully-dense, or very coarse-grained materials (wherein the machining crack may be entirely within one grain). On the other hand, they may be very difficult to detect in many polycrystalline ceramics since they often blend into the background microstructural features on the fracture surface. It is not uncommon for a fractographer to readily find a fracture mirror centered on a surface origin location, but not find an obvious defect at the origin. This has led some fractographers to *guess* that the origin must be machining damage. One objective of the present study was to refine techniques for finding machining cracks and to make their identification easier. Fractographic analysis entails pattern recognition. This study reveals some of the telltale features or patterns that can be detected with conventional optical microscopy. Ref. [1] is a comprehensive report on this study, which is copiously illustrated with examples and schematics of machining damage cracks. This paper summarized some of the key findings and presents a few illustrative examples for one particular sintered reaction-bonded silicon nitride.

Material

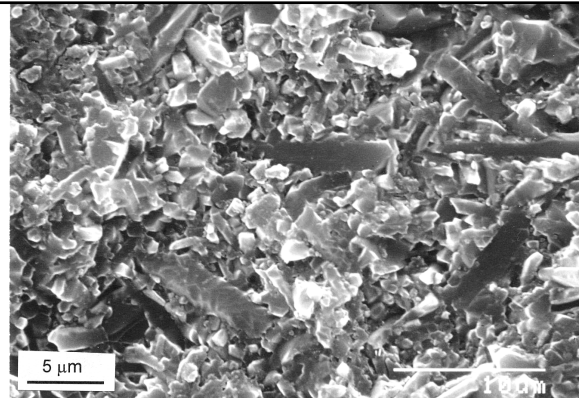
A sintered reaction-bonded silicon nitride (SRBSN)^{a,b} containing yttria and alumina was evaluated. The material is in full-scale production for several applications including cam roller followers in a diesel engine and pump valve components for the oil extraction industry. **Fig. 3** shows that this SRBSN has needle-like beta silicon nitride grains, 0.5 μm to 3 μm wide by up to 10 μm long, that are bonded by a second phase.

The material was designed to have enhanced fracture toughness. The manufacturer lists the elastic modulus as 310 GPa - 320 GPa, the strength as > 700 MPa, and density as 3.21 g/cm^3 . Silicon starting powders were isopressed into oversized green-body rods that were nitrided and then gas-pressure sintered. The rods were nominally 7.5 mm in diameter by 111 mm long after sintering. The fracture toughness of this material has been measured by the three methods in ASTM C 1421[14] and very consistent values were obtained. The surface crack in flexure (SCF) with Knoop semielliptical cracks as small as 50 μm and single-edged precracked beams (SEPB) methods gave values of 5.4 $\text{MPa}\sqrt{\text{m}} \pm 0.4 \text{MPa}\sqrt{\text{m}}$ and 5.6 $\text{MPa}\sqrt{\text{m}} \pm 0.2 \text{MPa}\sqrt{\text{m}}$, respectively [15]. Chevron notch (CN) testing [16] produced 5.3 $\text{MPa}\sqrt{\text{m}} \pm 0.2 \text{MPa}\sqrt{\text{m}}$.

^a Ceralloy 147-31N, Ceradyne, Cosa Mesa, CA.

^b Certain commercial materials or equipment are identified in this paper to specify adequately the experimental procedure. Such identification does not imply endorsement by the NIST nor does it imply that these materials or equipment are necessarily the best for the purpose.

Fig. 3 The SRBSN microstructure from a fracture surface.

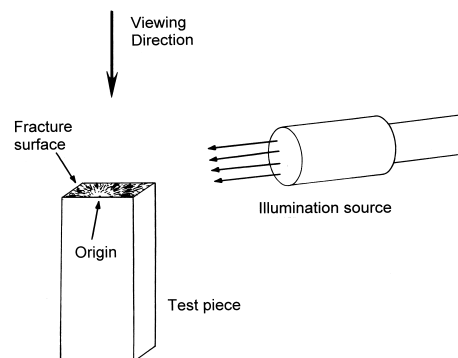
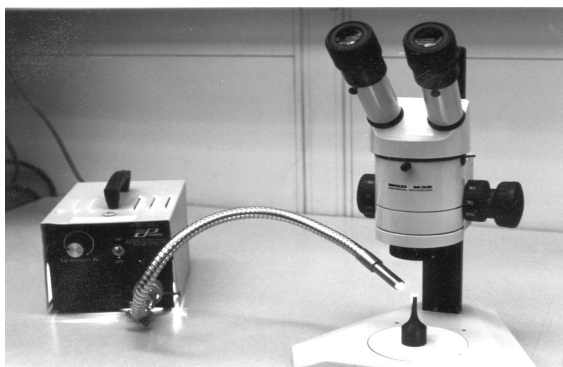


Experimental Procedure

Flexure testing with rod or rectangular bar specimens is an ideal method to accentuate surface machining flaws. Sample sets of 10 or 30 rod or bar specimens were prepared and tested per grinding condition. All cylindrical rods were 6.0 mm in diameter by 100 mm long. Rods were transversely- or longitudinally-ground with resin bonded diamond abrasive wheels with 150 to 600 grit sizes. Rods were tested on a four-point flexure fixture specifically designed for cylindrical rod specimens [4]. The spans were nominally 40 mm x 80 mm and the crosshead rate was 1.3 mm/min. All rectangular bars were “B” sized (3 mm x 4 mm x 45 mm) four-point flexure specimens and were prepared in accordance with ASTM C 1161 [17]. Specimens were either longitudinally- or transversely-ground with 80 to 600 grit wheels. The rods and bars were different in size but the Weibull effective volumes and effective surfaces were actually quite similar [18]. Additional experimental details are in Ref. [1].

The overall fractographic analysis was performed in accordance with ASTM C 1322 [19]. All fracture surfaces were examined with a stereo binocular microscope at magnifications up to 205X. It was essential to illuminate the specimen fracture surface from the side or rear with a bright, low incident angle (vicinal) illumination source as shown in **Fig. 4**. The low angle illumination accentuated many crucial tell tale features of machining damage. Many specimens were also examined with the scanning electron microscope. Optical microscopy was effective in finding and characterizing the machining cracks once we learned to recognize their telltale signs such as machining crack hackle. Illumination from directly above the specimen fracture surface was ineffective since it washed out many key features. Contrast was reduced and helpful shadows lost. Low angle illumination from the same side of the specimen that contained the machining cracks

Fig. 4 Stereo optical microscopy with vicinal (low angle) illumination.



w
edge at the origin. The SRBSN was partially translucent. The key to success was having a stereomicroscope that was capable of 100 X – 200 X magnifications and a bright directional illumination source. As the study progressed, and we gained greater experience in detecting the telltale features of machining damage cracks, we were able to speed up our inspection process and optimize our photography. By the end of the study, we could immediately identify transverse grinding damage on the first inspection with the stereomicroscope.

Results

Tables 1 and 2 list the rod and bar flexural strength outcomes. A detailed discussion of the strength data and a full Weibull statistical analysis are in Ref. [1]. Longitudinal grinding and finer grits led to the greatest strengths as expected. The 320 grit longitudinally-ground rod specimens had the greatest strengths and nearly all specimens broke from volume-distributed material flaws such as inclusions, porous zones, and second phase inhomogeneities. Many of the fracture origins were well into the rod interior. Three different machine shops (N, W, F) that participated in the project either matched this performance or came close with 600 grit centerless or transverse cylindrical grinding. Coarser wheel grits or more aggressive grinding procedures led to progressively deeper damage, specimen weakening, and a change of origins to machining cracks.

Table 1 SRBSN rod strength results and fractographic summary

SHOP	Specimen Preparation	Wheel Grit Depth of Cut Surface finish	Effect on Strength Average \pm std dev. (MPa)	Weibull parameters Char. Str. (MPa) Modulus, m	Primary Fracture Origins
C	Longitudinal (Centerless) 	320 grit 5 μm 0.45 $\mu\text{m} \pm 0.04 \mu\text{m}$	No effect "Baseline Strength" 816 \pm 59	843 m = 14.6	Inherent Volume Sintering Flaws: Inclusions, Compositional Inhomogeneities, Porous Regions, Large Grains 
N	Transverse 	600 grit 5 μm 0.054 $\mu\text{m} \pm 0.002 \mu\text{m}$	No effect. 806 \pm 49	827 m = 17.6	Parallel machining cracks Minor interaction with inherent flaws 
W	Transverse (cylindrical) 	600 grit 25 μm 0.14 $\mu\text{m} \pm 0.02 \mu\text{m}$	6% Reduction 764 \pm 55	789 m = 13.3	Parallel machining cracks Minor interaction with inherent flaws 
F	Transverse 	600 grit - 0.14 $\mu\text{m} \pm 0.02 \mu\text{m}$	10% Reduction 735 \pm 47	754 m = 18.9	Parallel machining cracks 13 - 20 μm deep Interaction with some inherent flaws 
C	Transverse 	320 grit 5 μm 0.24 $\mu\text{m} \pm 0.02 \mu\text{m}$	18% Reduction 670 \pm 32	686 m = 21.9	Flat coplanar parallel machining cracks 16 - 34 μm deep 
N	Transverse 	220 grit 5 μm -	28% reduction 589 \pm 22	600 m = 21.3	Long, parallel machining cracks 25 - 40 μm deep 
S	Transverse / Lapped 	30 μm grit - 0.074 $\mu\text{m} \pm 0.05 \mu\text{m}$	15-30% Reduction 628 \pm 76	? 660 m ? 7	"V" machining cracks from prior grinding 20 - 35 μm deep 
F	Transverse 	150 or 180 grit - 0.80 $\mu\text{m} \pm 0.06 \mu\text{m}$	48% reduction 427 \pm 14	433 m = 28.1	Coplanar parallel machining cracks; 40 - 80 μm deep; some V cracks 

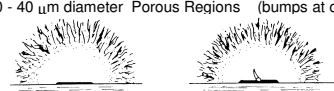
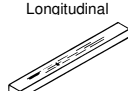
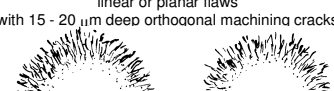
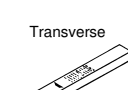
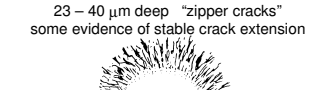
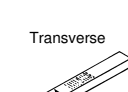
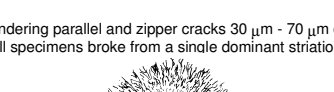
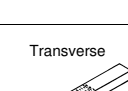
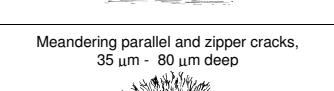
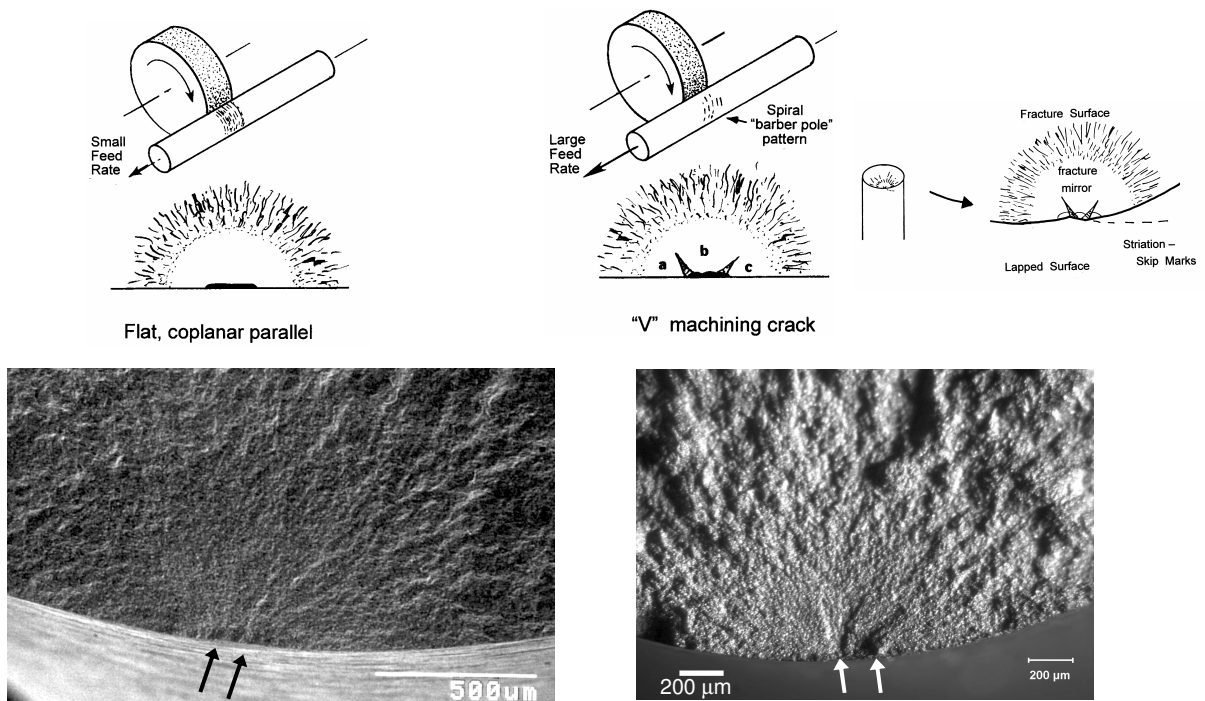
SHOP	Specimen Preparation	Wheel Grit Depth of cut Surface finish	Effect on Strength Average, std. dev. (MPa)	Weibull parameters Char. Str. (MPa) Modulus, m	Primary Fracture Origins
F	Transverse 	600 grit 5 μm ? 0.09 μm ± 0.01 μm	10% less than best rod strengths same strengths as their 600 grit rods. 726 ± 19	735 m = 36	12 – 18 μm deep parallel machining cracks, or 20 - 40 μm diameter Porous Regions (bumps at origin) 
C	Longitudinal 	320 grit ASTM C 1161 standard multi-step 5 μm 0.27 μm ± 0.01 μm	10% less than 600 grit, transverse bars above 20% less than best rods 655 ± 51	677 m = 15	Pores/Porous regions/Collapsed Agglomerates "linear or planar flaws" with 15 - 20 μm deep orthogonal machining cracks 
C	Transverse 	320 grit 5 μm 0.29 μm ± 0.02 μm	24% weaker than best 600 grit transverse bars above 550 ± 42	570 m = 12.5	23 – 40 μm deep "zipper cracks" some evidence of stable crack extension 
C	Transverse 	150 grit - -	37% weaker than best 600 grit transverse bars above 458 ± 72 2 sample lots	488 m = 6.8	Meandering parallel and zipper cracks 30 μm - 70 μm deep All specimens broke from a single dominant striation. 
F	Transverse 	80 grit - -	41% weaker than best 600 grit transverse bars above 430 ± 62 2 sample lots	443 m = 8.2	Meandering parallel and zipper cracks, 35 μm - 80 μm deep 

Fig. 5 Depending upon the axial feed rate, parallel machining cracks in rods may either be planar (on the left, SEM image), or segmented (on the right, optical image). Crack segments (a, b, c) link on different planes making the machining hackle that create the tell tale V pattern. Vicinal illumination helps the V stand out clearly despite the inherent roughness in the mirror region.



Final surface roughness did not correlate to strength [1]. For example, the lapped rods had the finest finish, but had some of the worst strengths since the flaws that controlled strength were from earlier phase grinding. The lack of a correlation between strength and surface finish in this SRBSN is consistent with findings from earlier phases of this project [2].

Figs. 5-7 show several key machining cracks and their tell tale features. Ref. [1] has almost one hundred pictures of machining cracks and material flaws in this silicon nitride.

Fig. 6 Two examples of “zipper cracks” in bend bars. A zipper crack is a parallel crack made up of a series of offset or zigzag crack segments. The segments link during fracture as the crack “unzippers” to the left and right along the surface. Offsets between the segments create the vertical “machining crack hackle” that extends up as fingers into the mirror region.

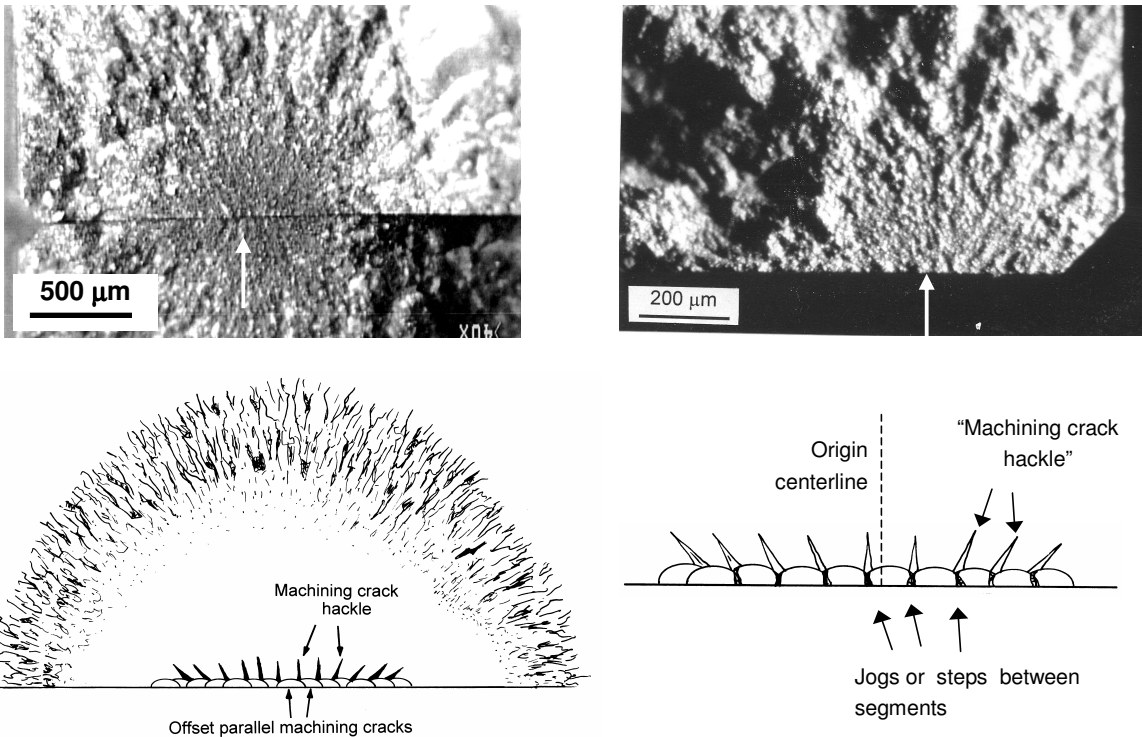
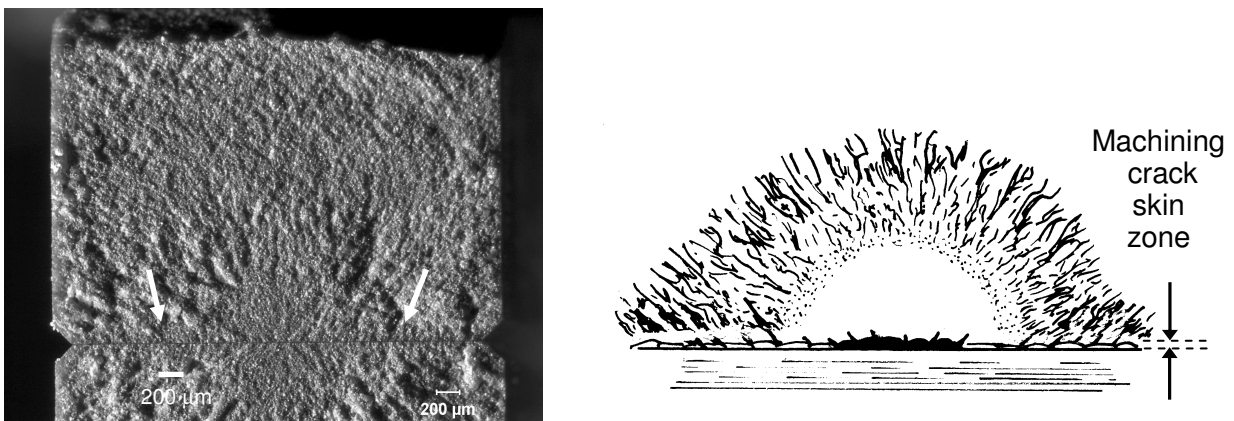


Fig. 7 Coarse grit (80, 150, 180) transverse grinding creates a damage zone along the surface (arrows). The damage zone has the same depth as the zipper crack at the origin.

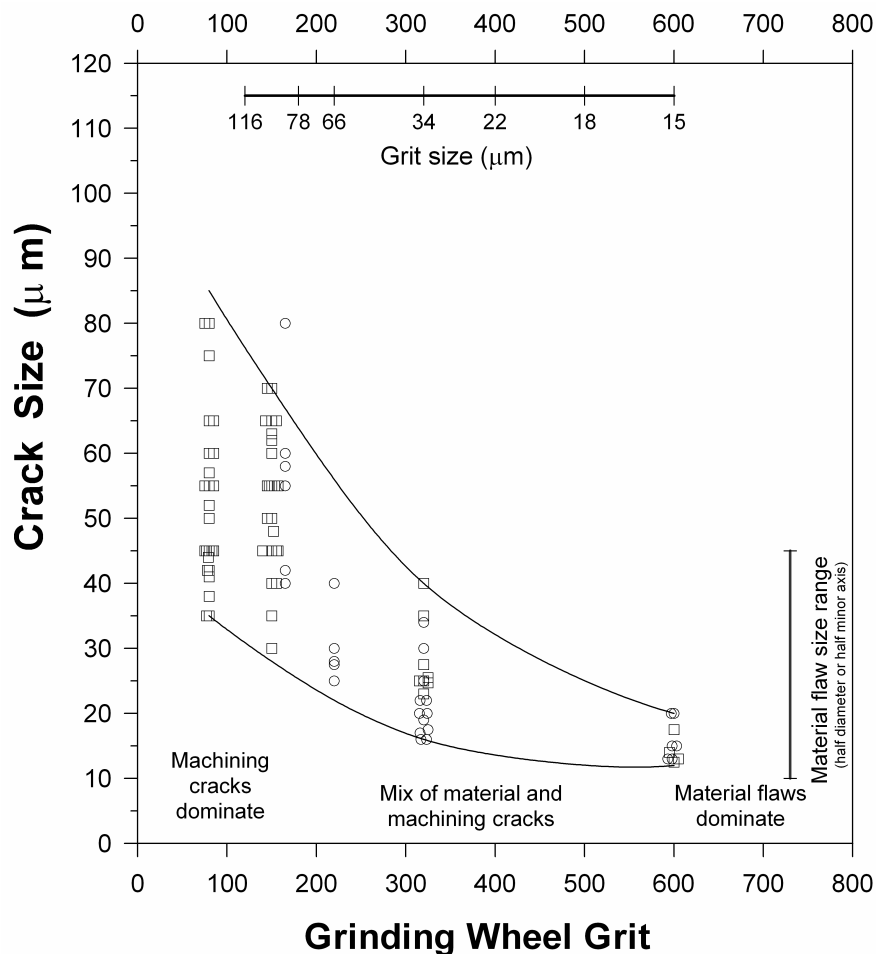


trend despite the fact that several machine shops participated in this exercise using different grinding machines and wheels. Crack depth is shown since it is the controlling dimension in fracture mechanics calculations for long shallow surface cracks in a body. The crack depth is also an important factor in assessing damage in a finished part. The critical crack size is shown. Only a few cracks showed evidence of stable extension and it was of the order of 5 μm to 15 μm . In each data set there are only some depth measurements since we were either unable to obtain a depth measurement in some specimens, or alternatively, the specimen may have fractured from a material flaw. The coarser the grit size, the more likely machining damage was strength limiting and the easier it was to measure the machining cracks.

The crack depths ranged from a minimum of 12 μm to a maximum of 80 μm . Sizes smaller than 12 μm do not appear since specimens with such small cracks broke from material flaws. The ≈ 80 μm upper limit corresponds to the severest machining damage likely to be encountered with conventional grinding conditions in this SRBSN. The surface lengths of the machining cracks varied from as low as ≈ 50 μm , to as long as hundreds of μm , to the full 4 mm width of the specimens in some of the coarsest ground (150 and 80 grit) bar specimens.

Several points may be made from Fig. 8. Firstly, there was good concurrence of crack depths for rods and bars at 600, 320, and 150/180 wheel grits. Secondly, despite the fact that specimens were ground by a number of different shops with many differences in key machining parameters

Fig. 8 The size (depth) of parallel machining cracks was strongly dependent upon the wheel grit size for transversely-ground rod (o) or rectangular (□) bar specimens.



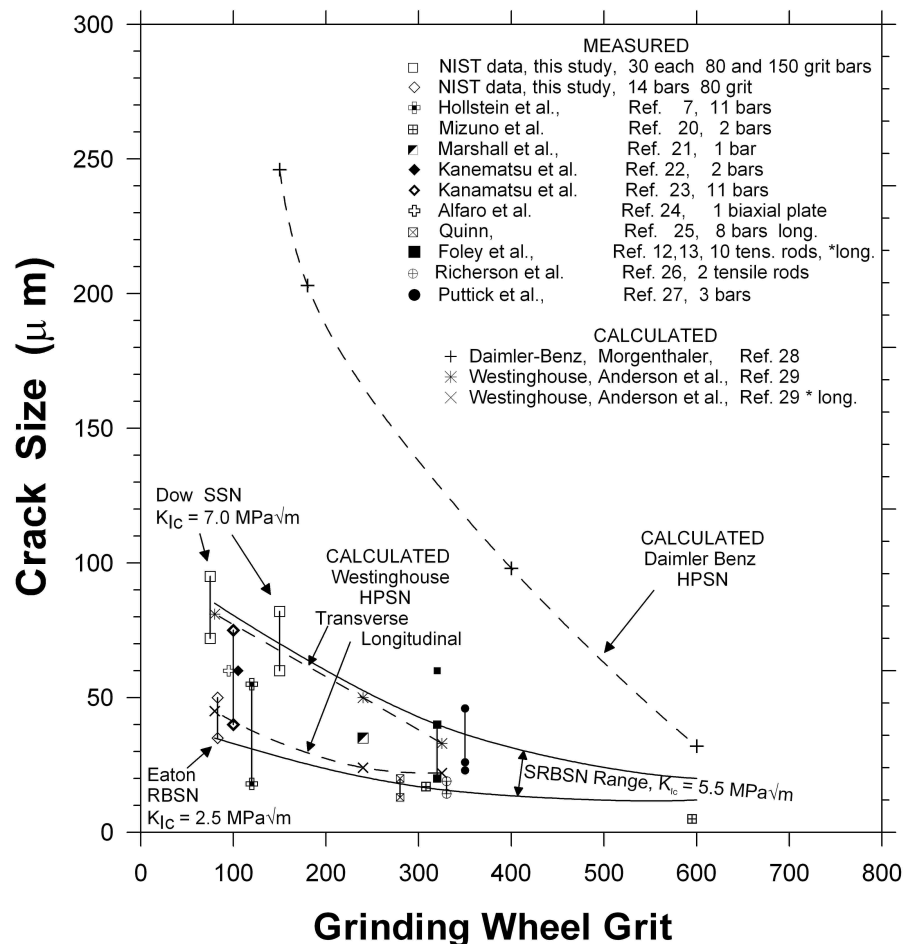
(€ grinding parameters had only a secondary effect. Thirdly, the range of machining crack sizes was of the order of a factor of two at each machining condition. Considering that strength scales with the inverse square root of crack size, the 2.0 factor is entirely consistent with the factor of 1.4 strength variation that was typical for the data sets.

Material flaws were dominant in the higher strength (> 600 MPa) specimens. A bar labeled with their size range ($10 \mu\text{m} - 45 \mu\text{m}$, half minor axis length) is on the right side of Fig. 8. Material flaws and machining cracks of the same size do not have the same severity. A sharp $20 \mu\text{m}$ deep machining crack is more deleterious than a rounded $20 \mu\text{m}$ radius ($40 \mu\text{m}$ diameter) pore. For the sample sets ground with 600 grit or 320 grit transverse wheels, some specimens broke from machining cracks, some from material flaws, and some from hybrid linked machining-material flaws. Machining flaws became dominant for grinding wheels coarser than 320 grit.

Fig. 9 shows how our data compare to that published by other groups for a variety of silicon nitrides [20,21,22,23,24,25,26,27,28,29]. The maximum machining crack depth detected in our study on the SRBSN was $80 \mu\text{m}$ under the coarsest grinding conditions. The maximum crack size for any silicon nitride from our review of other literature data was $\approx 100 \mu\text{m}$. An amazing finding is that nearly all data for silicon nitride fall within the bands shown in Fig. 6, except that the silicon nitrides with increased fracture toughness e.g., (Dow sintered silicon nitride – SSN) have larger machining cracks than in the untoughened silicon nitrides (e.g. Eaton reaction bonded silicon nitride - RBSN). This paradoxical finding is discussed in more detail in Ref. 1, but the reason is simple. Tougher silicon nitrides are more difficult to grind, but the grinding machine compensates by applying more force and energy to remove material. If the motor is powerful enough at a given set of conditions (wheel speed, depth of cut, wheel grit, etc), the grinder can drive the grinding cracks in deeper. **Fig. 10** is a simple summary diagram for damage depths in ground silicon nitride.

Fig. 10

The size (depth) of grinding cracks in a variety of silicon nitrides. All grinding was transverse unless otherwise noted by *long which means longitudinal. Nearly all the data fit the same trend.



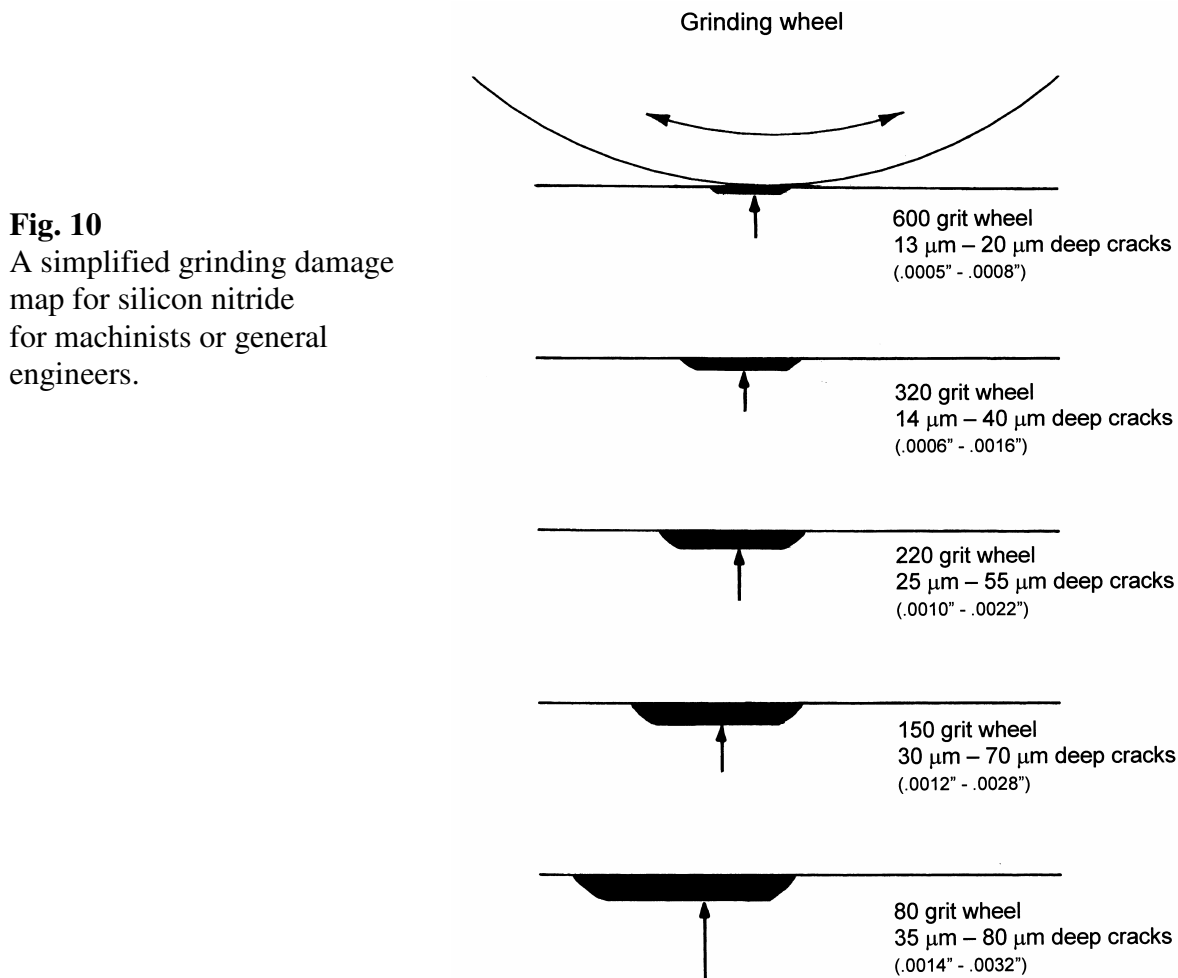


Fig. 10
A simplified grinding damage map for silicon nitride for machinists or general engineers.

An odd pattern occurred on several sets of coarse transversely-ground (80 and 150 grit) bars. Fracture always occurred from *one particular atypical striation*, which repeated itself along the bar length at regular intervals that corresponded to the table feed between grinding wheel passes. The deleterious striation was not the most obvious striation or the largest or deepest striation. It did have much more grain pull out, fracture, and fragmentation. The subsurface damage was manifested as light scattering sources beneath the surface. The striation appeared in the optical microscope as a fuzzy-blurred region rather than a distinct groove. In contrast, the other more noticeable striations on the tensile surface were grooves that suggested plastic deformation with negligible subsurface cracking. A simple calculation based on the specimen and wheel geometries and the table and wheel speeds indicated that a single abrasive grit might have formed the deleterious striation. Hence, one “renegade” abrasive grit in the grinding wheel may control the strength.

The grinding flaws in rods and bars were similar in some respects, but different in others. The trends of crack depths for the rods and bars were similar, but the crack lengths varied. This difference is not surprising due to the geometries and the shorter contact length and duration of a round rod contacting a round grinding wheel. Rectangular bars typically had longer machining cracks, often in the hundreds of μm and sometimes the full 4 mm width of the specimen. The bars were more likely to have “zipper cracks” with periodic fingerlets and machining crack hackle. The

rc

motion of the work piece relative to the grinding wheel.

A number of the machining cracks had sufficiently well defined shapes and boundaries that apparent critical fracture toughness could be computed from the measured crack depth and width, the stress at the origin, and the computed stress intensity shape factor. The average for 29 cracks was $5.41 \text{ MPa}\sqrt{\text{m}} \pm 0.54 \text{ MPa}\sqrt{\text{m}}$ which matched $5.5 \text{ MPa}\sqrt{\text{m}}$ grand average for the data collected by the three test methods in the ASTM fracture toughness standard C 1421. One of the three methods was the surface crack in flexure (SCF) method that used a Knoop indenter to make small semi elliptical surface cracks which are very close in size ($50 \mu\text{m}$) to some of the machining cracks.

As noted above, a few SRBSN machining cracks showed evidence of small amounts ($5 \mu\text{m} - 15 \mu\text{m}$) of stable crack extension, but most did not. The critical crack size was used in the calculations. We could often distinguish the critical crack on the fracture surface by noting where the flaw topography changed to a flatter final fracture plane and also by observing changes in direction of machining hackle lines. The latter show the local direction of crack extension. It could not be ascertained whether the stable extension was due to residual stresses, R-curve toughening, or stepwise pop in during the initial grinding.

Any R-curve toughening in this material occurred over very short crack extensions of the order of $5 \mu\text{m} - 15 \mu\text{m}$ at most, since the computed fracture toughness from the critical crack sizes matched the outcomes from the SEPB, CNB, and SCF outcomes cited earlier. The SCF experiments with residual stress-free $50 \mu\text{m}$ deep Knoop cracks did not detect any greater extensions either.

An absence of residual stresses could be inferred from the fracture mechanics analysis of the machining cracks. The computed fracture toughness (based on applied flexure stress at fracture) usually matched the known fracture toughness, suggesting that residual stresses were small.

Figs. 11 and 12 summarize some of the tell tale features of machining cracks and are based on the observations of hundreds of flaws in this study, plus our experience with other ceramics and glasses.

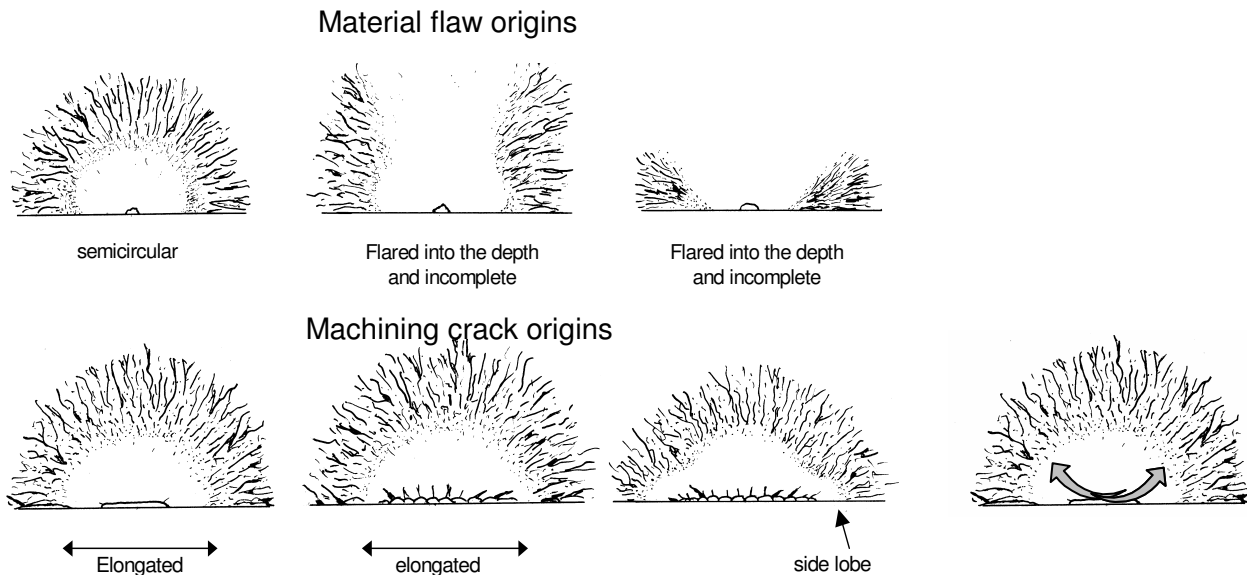


Fig. 11 Schematics of fracture mirror shapes and distortions. The top row shows mirrors centered on origins such as inclusions or pores. Mirror elongations into the depth are common in flexure specimens. Alternatively, long parallel machining cracks cause mirrors that are elongated along the surface. The insert on the right shows how the mirror elongations may develop.

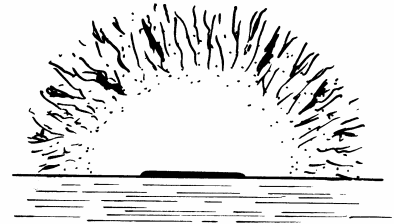
F

biaxial disks, flexural, and tension strength specimens, or transversely-ground components.

(a) elongated “coplanar parallel crack”

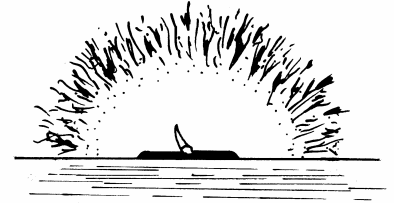
(or coplanar linked semi-elliptical cracks).

A deep striation may or may not necessarily be present. The fracture mirror may be elongated along the outer specimen surface.

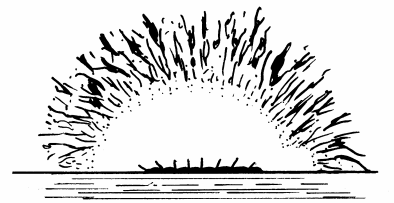
**(b) elongated “coplanar parallel crack”**

linked with a material flaw.

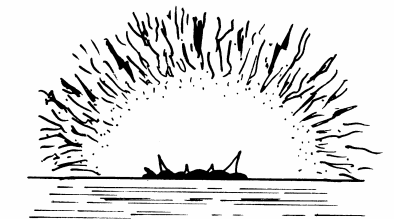
A step in the fracture origin emanates from the material flaw.

**(c) “zipper crack”**

This is a parallel crack made by a series of short semi elliptical cracks, which have linked. A series of short tails, or “machining crack hackle,” emanate from the links or overlaps of the flaws and extend up into the fracture mirror. These tails may be tilted to the left or right and help confirm that fracture originated in the central region of the set. The short tails are telltale features of slightly misaligned or overlapping transverse machining cracks (or a scratch) and are often easier to see with an optical microscope with low angle lighting than with a scanning electron microscope. The fracture mirror may be elongated along the specimen outer surface or it may have one or two prominent side lobes. This origin type is common in transversely-ground rectangular flexure specimens or scratched biaxial disk specimens.

**(d) coarse “zipper crack”**

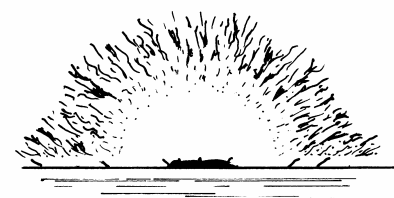
This is a parallel crack made up of a series of irregular, less coplanar semi-elliptical cracks. Larger tails than in (c) are created. In severe cases, the tail may extend all the way to the mirror boundary. The fracture mirror may be elongated. This origin is common in transversely ground or scratched specimens and the markings are sometimes termed “shark’s teeth.”

**(e) “V machining crack”**

The crack intersects the fracture surface at an angle. Only a portion of the machining crack or crack series is exposed. A pronounced step occurs in the fracture mirror. One or two (shown) tails extend well up into the fracture mirror. The machining direction is not quite perpendicular to the specimen length and uniaxial stress axis due to grinding wheel cross feed. This origin is common in cylindrical specimens prepared by centerless or cylindrical transverse grinding wherein the wheel and work piece displace axially relative to each other.

**(f) “coarse grinding parallel crack”**

The origin is a deep machining crack that extends side-to-side across the entire surface. The origin is often bumpy since the origin is comprised of offset parallel cracks. Thin bands of uniform depth extend along the specimen surface on either side of the fracture mirror. The bands have the same depth as the grinding cracks. Short tails, or “machining crack hackle” which may be in the thin bands are tilted away from the origin. This origin is common in coarse ground surfaces.



Numerous machining cracks were characterized in a commercial, toughened silicon nitride. The dominant factors in determining flaw severity were the abrasive wheel grit size and the direction of machining. The depth of machining cracks correlated strongly with the wheel grit. Cracks were as shallow as 12 μm for 600 grit ground surfaces to as deep as 80 μm for 80 grit transverse ground surfaces. A literature review indicated that $\approx 100 \mu\text{m}$ may be an upper limit for the depth of machining cracks in ground silicon nitride. For a given set of test specimens that were ground at the same time by the same machine and wheel, the crack size variability from specimen to specimen was a factor of two. This variability matched the strength variability.

The SRBSN's "inherent material strength," whereby specimens nearly all fractured from material flaws, was obtained from rods ground longitudinally with a 320 grit wheel. Three shops matched or came close to matching this performance with 600 grit centerless or transverse cylindrical grinding.

Cylindrical and centerless grinding may create similar, but not necessarily identical, flaws in rods than those created in surface ground flat bend bars.

Strength limiting machining cracks sometimes were associated with particular striations that were not necessarily the deepest or most obvious on the ground surface. A single "renegade" abrasive grit in a diamond wheel may control performance.

Machining cracks flaws in this SRBSN experience a resistance to fracture commensurate with plateau fracture toughness values. Evidently the benefits of the enhanced fracture toughness due to the interlocking grain microstructure occur during crack initiation or pop in. Subsequent stable crack extensions are small.

Simple optical microscopy techniques may be used to detect machining damage. The telltale fracture markings for detecting machining are tabulated in a series of schematic drawings, which will help engineers and analysts find and characterize machining damage flaws with greater confidence.

Acknowledgements

The authors thank Dr. B. Mikijelj of Ceradyne Inc., Mr. Richard Allor of Ford Motor Company, and Dr. Ron Chand of Chand-Kare Technical Ceramics. Partial support for this project was furnished by the U. S. Department of Energy, Office of Transportation Technologies.

References

- [1] G.D. Quinn, L.K. Ives, and S. Jahanmir: NIST Special Publication 996, (NIST, Gaithersburg, MD, 2003, Available from the author).
- [2] S. Jahanmir, T. Strakna, G. D. Quinn, H. Liang, R. Allor, and R. West: pp. 263-278 in *Machining of Advanced Materials*, ed. S. Jahanmir, NIST Special Publication 847, (NIST, Gaithersburg, MD, 1993).
- [3] S. Jahanmir, T. Strakna, G.D. Quinn, R. Kopp, S. Yoon, K. Kumar: *ibid*, pp. 279-294.
- [4] G.D. Quinn, L. K. Ives, S. Jahanmir, and P. Koshy: pp. 343 – 365 in *Fractography of Glasses and Ceramics IV*, Ceramic Transactions, Vol. 122, eds, J. Varner and G. Quinn, (American Ceramic Society, Westerville, OH, 2001).
- [5] H.K. Xu, S. Jahanmir, and L.K. Ives: *J. Mater. Res.*, Vol. 11 [7] (1996), pp. 1717-1724.
- [6] H.K. Xu, L. Wei, and S. Jahanmir: *ibid*, Vol. 10 [12] (1995), pp. 3204-3209.
- [7] T. Hollstein, W. Pfeiffer, M. Rombach, and B. Thielicke: pp. 145-169 in *Fractography of Glasses and Ceramics, III*, Ceramic Transactions, Vol. 64, eds. J. Varner, V. Fréchette and G. Quinn, (ACS, Westerville, OH, 1996).

-
- [8] R.W. Rice and J.J. Mecholsky, Jr.: pp. 351- 378 in *The Science of Ceramic Machining and Surface Finishing II*, eds. B.J. Hockey and R.W. Rice, National Bureau of Standards Special Publication 562, (NIST, Gaithersburg, MD, 1979).
- [9] R.W. Rice, J.J. Mecholsky, Jr., and P.F. Becher: *J. Mat. Sci.*, Vol. 16 (1981), pp. 853-862.
- [10] J.J. Mecholsky, Jr., S.W. Freiman, and R.W. Rice: *J. Amer. Ceram. Soc.*, Vol. 60 [3-4] (1997), pp. 114-117.
- [11] R.W. Rice: pp. 223-234 in *Machining of Advanced Materials*, ed. S. Jahanmir, NIST SP 847, (NIST, Gaithersburg, MD, 1993).
- [12] M.R. Foley, V.K. Pujari, L.C. Sales, and D.M. Tracey: pp. 3 -18 in *Life Prediction Methodologies and Data for Ceramic Materials*, ASTM STP 1201, eds. C.R. Brinkman and S.F. Duffy, (ASTM, West Conshohocken, PA, 1994).
- [13] V.K. Pujari, D.M. Tracey, M.R. Foley, N.I. Paille, P.J. Pelletier, L.C. Sales, C.A. Wilkins, and R.L. Yeckley: Oak Ridge National Laboratory Technical Report, ORNL/Sub/89-SB182/1, Aug. (1983).
- [14] ASTM C 1421-99, *ASTM Annual Book of Standards*, Vol. 15.01, (ASTM, West Conshohocken, PA, 2001).
- [15] G. D. Quinn, J.J. Swab, and M. Motyka: *J. Am. Ceram. Soc.*, 86 [6] (2003), pp. 1043-1045.
- [16] B. Mikijelj: private communication, (2000).
- [17] ASTM C 1161-02, *ASTM Annual Book of Standards*, Vol. 15.01, (2002).
- [18] G. D. Quinn: *J. Am. Ceram. Soc.*, Vol. 86 [3] (2003), pp. 475-478.
- [19] ASTM C 1322-02, *ASTM Annual Book of Standards*, Vol. 15.01, (2002).
- [20] S. Mizuno, N. Kobayashi, and K. Miyata: Society of Automotive Engineers paper 930163, (SAE, Warrendale, PA, 1993).
- [21] D.B. Marshall, A.G. Evans, B.T. Khuri Yakub, J.W. Tien, and G.S. Kino: *Proc. Roy. Soc. Lond.*, Vol. A 385 (1983), pp. 461- 475.
- [22] W. Kanematsu, M. Sando, L.K. Ives, R. Marinenko, and G. D. Quinn: *J. Amer. Ceram. Soc.*, Vol. 84 [4] (2001), pp. 795-800.
- [23] W. Kanematsu and L. K. Ives: *ibid*, Vol. 87 [3] (2004), pp. 500 – 503.
- [24] E.S. Alfaro, J.V. Guiheen, and J.R. Varner: pp. 485-508 in *Fractography of Glasses and Ceramics, II*, eds. V.D. Fréchette and J.R. Varner, Ceramic Transactions, Vol. 17, (American Ceramic Society, Westerville, OH, 1991).
- [25] G. D. Quinn: Unpublished Research, Watertown Arsenal, Watertown, MA, 1980.
- [26] D.W. Richerson, T.M. Yonushonis, and G.Q. Weaver: pp. 193-218 in *Proceedings of the 1977 DARPA/NAVSEA Ceramic Gas Turbine Demonstration Engine Program Review*, Castine, Maine, eds., J.J. Fairbanks and R.W. Rice, Metals and Ceramics Information Center MCIC Report 78-36, Battelle, Columbus, OH, March, 1978.
- [27] K.E. Puttick, M.R. Rudman, M.A. Kirwan, R. Quinn, and G. Syers: *J. Hard Mater.*, Vol. 4 (1993), pp. 55-76.
- [28] K. Mörgenthaler: Private Communication, 1989.
- [29] C.A. Anderson and R.J. Bratton: pp. 463 –476 in *The Science of Ceramic Machining and Surface Finishing II*, eds. B.J. Hockey and R.W. Rice, National Bureau of Standards Special Publication 562, Gaithersburg, MD, 1979.